Supplementary Information: Hydrogen Adsorption in the Metal-Organic Frameworks Fe_2(dobdc) and $Fe_2(O_2)$(dobdc)

Table S1: Rietveld Refinement (4 K data) of the Fe_2(dobdc) loaded with 0.75 D_2 molecules per iron site. a = 26.095(3)Å, c = 6.894(1)Å, and V = 4065.8(8)Å^3

Atom	X	Y	Z	Multiplicity	Occupancy	Uiso (Å^2)
Fe	0.3820(8)	0.3514(9)	0.142(3)	18	1.0	0.035(6)
O1	0.320(1)	0.286(1)	0.366(4)	18	1.0	0.00(1)
O2	0.302(1)	0.229(1)	0.600(4)	18	1.0	0.00(1)
O3	0.357(2)	0.270(1)	0.010(5)	18	1.0	0.028(9)
C1	0.312(2)	0.241(2)	0.442(5)	18	1.0	0.09(1)
C2	0.329(1)	0.209(1)	0.282(4)	18	1.0	0.014(8)
C3	0.343(1)	0.221(1)	0.076(4)	18	1.0	0.018(8)
C4	0.353(1)	0.178(1)	-0.028(3)	18	1.0	0.005(7)
H	0.369(2)	0.200(2)	-0.173(8)	18	1.0	0.03(1)
D1	0.531(1)	0.6529(8)	0.746(3)	18	1.33(5)	0.03(1)

Table S2: Rietveld Refinement (4 K data) of the Fe_2(dobdc) loaded with 2.25 D_2 molecules per iron site. a = 26.102(3) Å, c = 6.911(1) Å, and V = 4077.6(9) Å^3

Atom	X	Y	Z	Multiplicity	Occupancy	Uiso (Å^2)
Fe	0.3818(8)	0.3513(9)	0.141(3)	18	1.0	0.008(7)
O1	0.318(2)	0.285(2)	0.353(5)	18	1.0	0.01(1)
O2	0.300(2)	0.231(2)	0.598(6)	18	1.0	0.01(1)
O3	0.354(2)	0.271(2)	0.011(7)	18	1.0	0.04(1)
C1	0.312(2)	0.244(2)	0.445(5)	18	1.0	0.05(1)
C2	0.328(1)	0.208(1)	0.279(5)	18	1.0	0.01(1)
C3	0.342(1)	0.221(1)	0.086(5)	18	1.0	0.00(1)
C4	0.353(1)	0.179(2)	-0.028(4)	18	1.0	0.01(1)
H	0.369(3)	0.1200(3)	-0.18(1)	18	1.0	0.04(2)
D1	0.534(1)	0.654(1)	0.747(3)	18	1.54(8)	0.03(1)
D2	0.452(1)	0.295(2)	0.663(4)	18	1.31(8)	0.113*
D3	0.235(1)	0.486(1)	0.857(5)	18	1.47(6)	0.110*

Uaniso D2 = [U_{11},U_{12},U_{13},U_{22},U_{23},U_{33}] = [0.07(4) 0.10(4) -0.06(3) 0.25(5) -0.02(3) 0.05(3)]
Uaniso D3 = [U_{11},U_{12},U_{13},U_{22},U_{23},U_{33}] = [0.01(2) 0.05(2) 0.05(2) 0.12(3) 0.05(3) 0.22(5)]

Table S3: Rietveld Refinement (4 K data) of the $Fe_2(O_2)$(dobdc) loaded with 0.25 D_2 molecules per iron site. a = 25.969(2) Å, c = 6.8209(9) Å, and V = 3983.6(6) Å^3

Atom	X	Y	Z	Multiplicity	Occupancy	Uiso (Å^2)
Fe	0.3801(5)	0.3468(6)	0.138(2)	18	1.0	0.022(4)
O1	0.3273(8)	0.2982(8)	0.359(3)	18	1.0	0.048(9)
O2	0.308(1)	0.223(1)	0.608(3)	18	1.0	0.040(7)
O3	0.3510(8)	0.2706(5)	0.001(3)	18	1.0	0.032(7)
C1	0.316(1)	0.2469(8)	0.410(2)	18	1.0	0.046(7)
C2	0.336(1)	0.2120(9)	0.284(3)	18	1.0	0.053(9)
C3	0.3477(9)	0.2243(8)	0.077(3)	18	1.0	0.017(5)
C4	0.3576(9)	0.1790(9)	-0.016(3)	18	1.0	0.029(6)
H	0.368(2)	0.189(2)	-0.198(5)	18	1.0	0.03(1)
O1a	0.529(1)	0.613(2	0.725(5)	18	0.53(6)	0.03(2)
O1b	0.519(4)	0.635(5)	0.93(1)	18	0.53(6)	0.464*
D1	0.541(3)	0.666(3)	0.686(9)	18	0.53(8)	0.05(3)

Uaniso=[U_{11},U_{12},U_{13},U_{22},U_{23},U_{33}] = [0.3(2), 0.1(1), 0.4(2), 0.3(2), 0.2(2), 0.8(3)]

Table S4: Rietveld Refinement (4 K data) of the $Fe_2(O_2)$(dobdc) loaded with O.5 D_2 molecules per iron site a = 25.961(1) Å, c = 6.8377(7) Å, and V = 3991.1(5) Å^3

Atom	X	Y	Z	Multiplicity	Occupancy	Uiso (Å^2)
Fe	0.3810(4)	0.3479(5)	0.135(1)	18	1.0	0.022(3)
O1	0.3276(8)	0.2996(7)	0.350(3)	18	1.0	0.049(9)
O2	0.3032(9)	0.220(1)	0.602(2)	18	1.0	0.032(7)
O3	0.3532(7)	0.2721(4)	0.001(3)	18	1.0	0.009(5)
C1	0.314(1)	0.2468(7)	0.409(2)	18	1.0	0.037(6)
C2	0.332(1)	0.2114(8)	0.289(2)	18	1.0	0.045(8)
C3	0.3444(8)	0.2236(8)	0.083(2)	18	1.0	0.009(4)
C4	0.3527(9)	0.1783(9)	-0.015(2)	18	1.0	0.019(5)
H	0.367(1)	0.193(1)	-0.1725(2)	18	1.0	0.008(8)
O1a	0.530(2)	0.617(2)	0.721(5)	18	0.54(6)	0.017(2)
O1b	0.511(4)	0.618(5)	0.940(8)	18	0.54(6)	0.531
D1b	0.531(2)	0.659(2)	0.721(4)	18	0.9(1)	0.06(2)
D1a	0.577(5)	0.691(5)	0.61(2)	18	0.39(8)	0.13(5)

Uaniso=[U_{11},U_{12},U_{13},U_{22},U_{23},U_{33}] = [0.2(1), 0.1(1), 0.4(2), 0.5(2), 0.4(2), 0.8(3)]

Table S5: Rietveld Refinement (10 K data) of the Fe_2(dobdc) loaded with 1.0 D_2 molecules per iron site. a = 25.957(1)Å, c = 6.8430(8)Å, and V = 3992.9(5) $Å^3$

Atom	X	Y	Z	Multiplicity	Occupancy	Uiso ($Å^2$)
Fe	0.3809(4)	0.3480(5)	0.141(2)	18	1.0	0.030(3)
O1	0.3251(6)	0.2982(6)	0.347(2)	18	1.0	0.008(6)
O2	0.3029(8)	0.222(1)	0.602(2)	18	1.0	0.030(7)
O3	0.3514(6)	0.2714(4)	0.009(2)	18	1.0	0.015(6)
C1	0.3155(9)	0.2467(6)	0.405(2)	18	1.0	0.020(5)
C2	0.334(1)	0.211(1)	0.292(3)	18	1.0	0.071(9)
C3	0.3442(8)	0.2237(7)	0.087(3)	18	1.0	0.013(4)
C4	0.351(1)	0.1796(9)	-0.024(2)	18	1.0	0.029(6)
H	0.365(1)	0.192(1)	-0.180(3)	18	1.0	0.003(8)
O1a	0.531(2)	0.612(2)	0.714(6)	18	0.45(2)	0.004(6)
O1b	0.515(6)	0.629(7)	0.92(2)	18	0.45(2)	0.504*
D1	0.535(1)	0.660(1)	0.714(3)	18	1.61(6)	0.197*
D2	0.536(3)	0.686(4)	0.36(1)	18	0.72(5)	0.540*

Uaniso O1b =$[U_{11},U_{12},U_{13},U_{22},U_{23},U_{33}]$ = [0.3(2), 0.2(1), 0.1(2), 0.4(2), -0.02(2), 0.8(3)]
Uaniso D1 =$[U_{11},U_{12},U_{13},U_{22},U_{23},U_{33}]$ = [0.26(4), 0.14(3), -0.05(2), 0.17(2), -0.05(2), 0.21(2)]
Uaniso D2 =$[U_{11},U_{12},U_{13},U_{22},U_{23},U_{33}]$ = [0.6(2), 0.4(2), -0.1(2), 0.7(1), -0.1(1), 0.4(1)]

Table S6: Rietveld Refinement (10 K data) of the $Fe_2(O_2)$(dobdc) loaded with 2.0 D_2 molecules per iron site. a = 25.954(2) Å, c = 6.8539(9) Å, and V = 3998.3(6) $Å^3$

Atom	X	Y	Z	Multiplicity	Occupancy	Uiso ($Å^2$)
Fe	0.3800(4)	0.3480(6)	0.144(2)	18	1.0	0.041(4)
O1	0.3250(9)	0.2957(7)	0.348(3)	18	1.0	0.024(9)
O2	0.3031(9)	0.226(1)	0.602(2)	18	1.0	0.008(7)
O3	0.3512(7)	0.2720(4)	0.010(3)	18	1.0	0.003(6)
C1	0.316(1)	0.2441(9)	0.400(2)	18	1.0	0.045(9)
C2	0.330(2)	0.205(1)	0.288(3)	18	1.0	0.07(1)
C3	0.346(1)	0.2258(8)	0.092(3)	18	1.0	0.008(5)
C4	0.353(1)	0.1835(9)	-0.028(3)	18	1.0	0.017(7)
H	0.370(2)	0.194(2)	-0.185(3)	18	1.0	0.001(9)
O1a	0.532(1)	0.609(2)	0.716(4)	18	0.44(3)	0.001(1)
O1b	0.515(5)	0.632(5)	0.902(9)	18	0.44(3)	0.653*
D1	0.536(2)	0.655(2)	0.734(4)	18	1.78(8)	0.226*
D2	0.5419(9)	0.697(1)	0.315(5)	18	2.02(9)	0.237*
D3	0.232(4)	0.492(5)	0.85(2)	18	0.31(5)	0.116*

Uaniso O1b =$[U_{11},U_{12},U_{13},U_{22},U_{23},U_{33}]$ = [0.8(4), 0.4(4), 0.2(3), 0.8(3), 0.0(3), 0.4(4)]
Uaniso D1 =$[U_{11},U_{12},U_{13},U_{22},U_{23},U_{33}]$ = [0.21(4), 0.06(3), 0.01(3), 0.19(4), -0.00(3), 0.23(5)]
Uaniso D2 =$[U_{11},U_{12},U_{13},U_{22},U_{23},U_{33}]$ = [0.22(3), 0.15(3), -0.02(3), 0.26(4), 0.04(3), 0.28(4)]
Uaniso D3 =$[U_{11},U_{12},U_{13},U_{22},U_{23},U_{33}]$ = [0.01(8), 0.0(1), -0.09(6), 0.2(2), -0.06(9), 0.1(1)]

Figure S1: Excess H_2 adsorption isotherms collected for Fe_2(dobdc) (green) and $Fe_2(O_2)$(dobdc) (black) at 87 K. Filled and open circles represent adsorption and desorption, respectively.

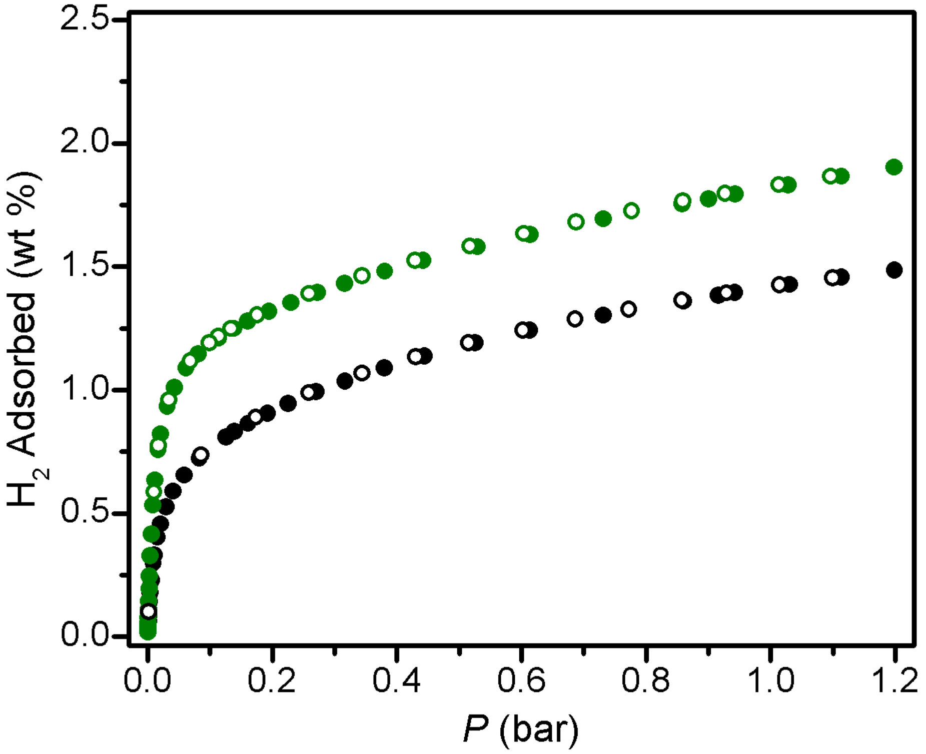

Figure S2: Occupancy of site **I** (red) and **II** (black) plotted as a function of temperature for 4 different D_2 loadings in Fe_2(dobdc) including (A) 0.5, (B) 1.0, (C) 1.5, and (D) 2.0 D_2 molecules per Fe^{2+}. The data were acquired from a high-flux neutron powder diffractometer, Wombat.

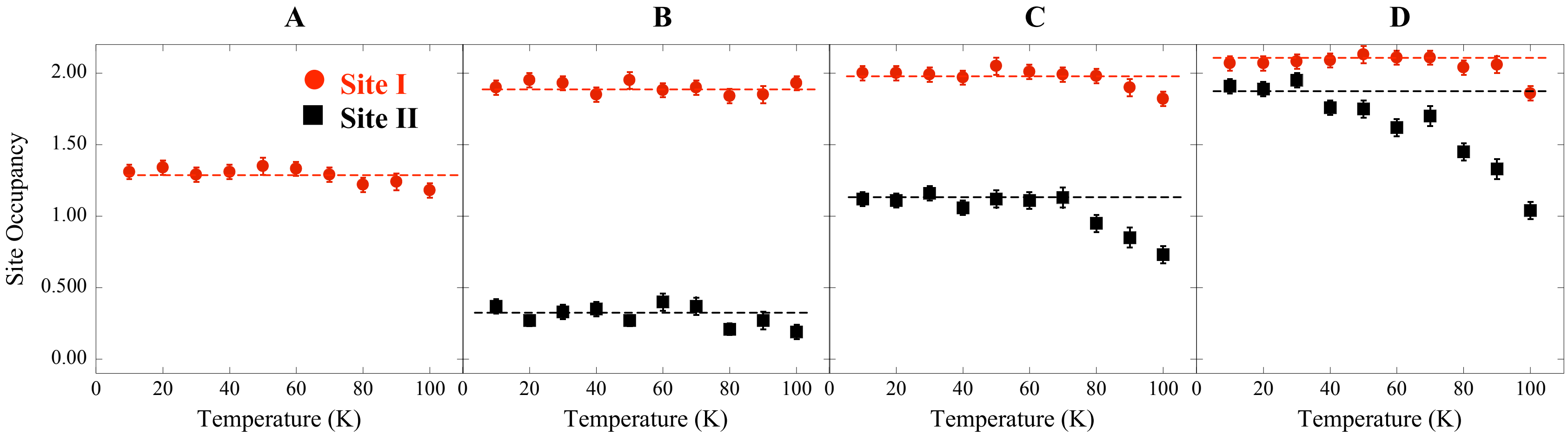

Figure S3: Unit cell volume of Fe_2(dobdc) plotted as a function of D_2 loading at 10 K (red spheres) and 100 K (black spheres). Error bars represent a single standard deviation. The data were collected using a high flux powder neutron diffractometer, Wombat.

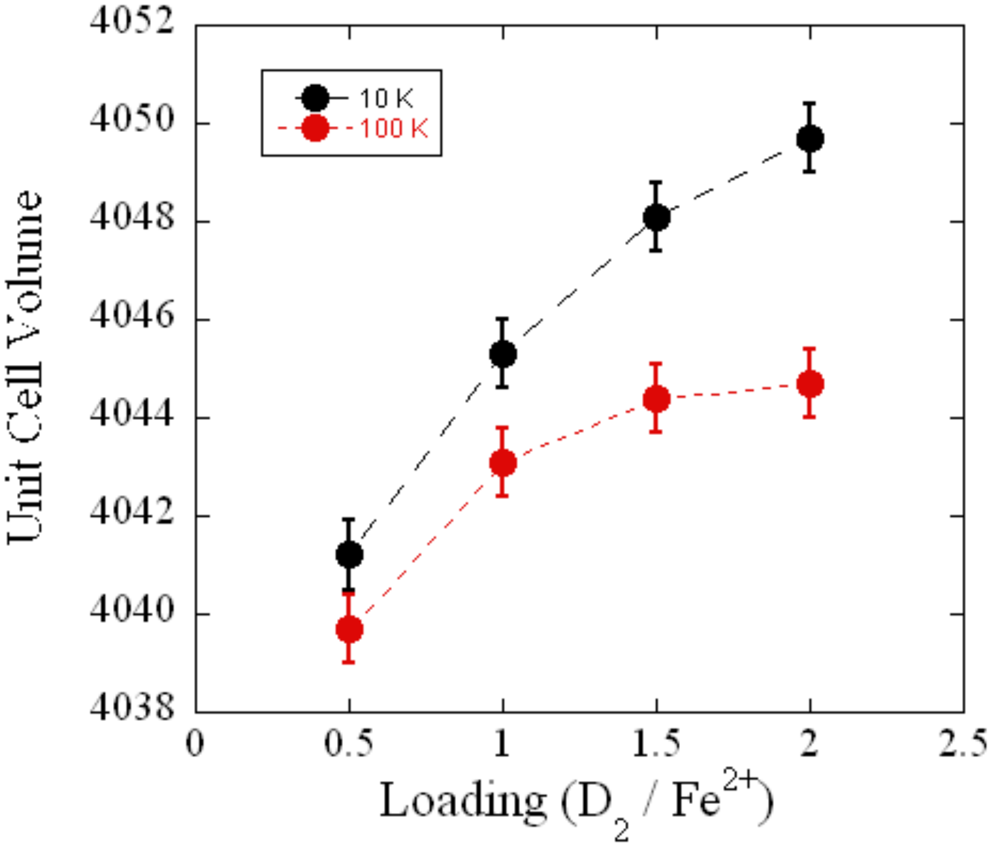

Figure S4: INS spectra recorded at 4 K (from the FANS spectrometer) for loadings of 0.1 (black), 0.25 (red), 0.5 (green), 1.0 (blue), and 1.5 (brown), *n*-H_2 molecules per Fe^{2+} in Fe_2(dobdc). The data were obtained following subtraction of the spectrum obtained from the evacuated sample.

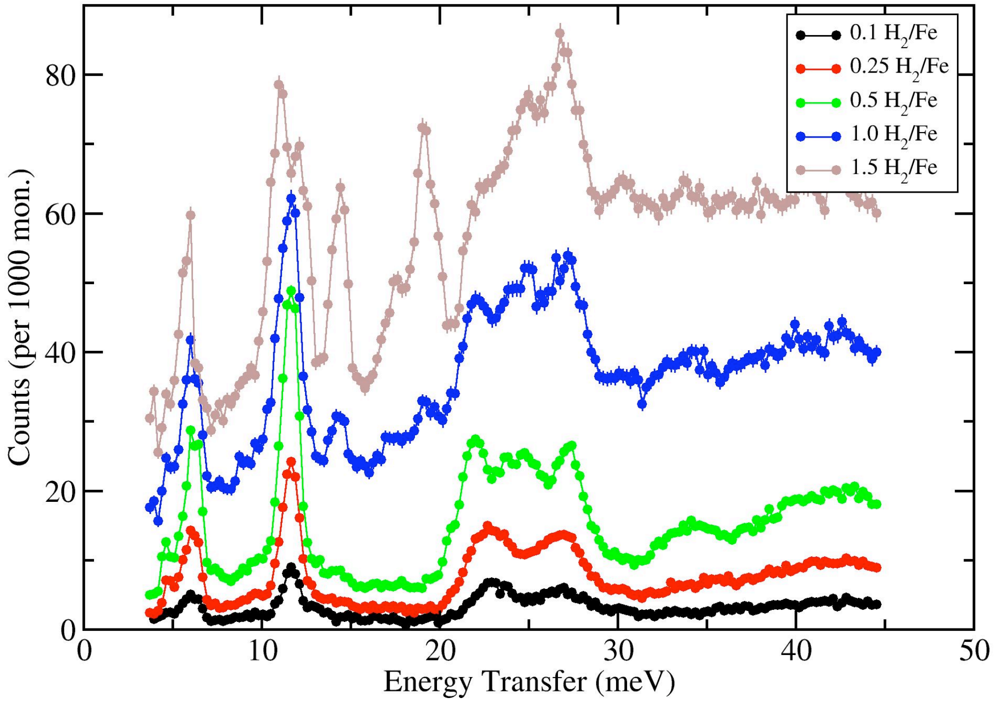

Figure S5: INS spectra recorded at 4 K (from the TOSCA spectrometer) for loadings of 0.5 to 3.75 *p*-H_2 molecules per Fe^{2+} in Fe_2(dobdc). The data were obtained following subtraction of the spectrum obtained from the evacuated sample.

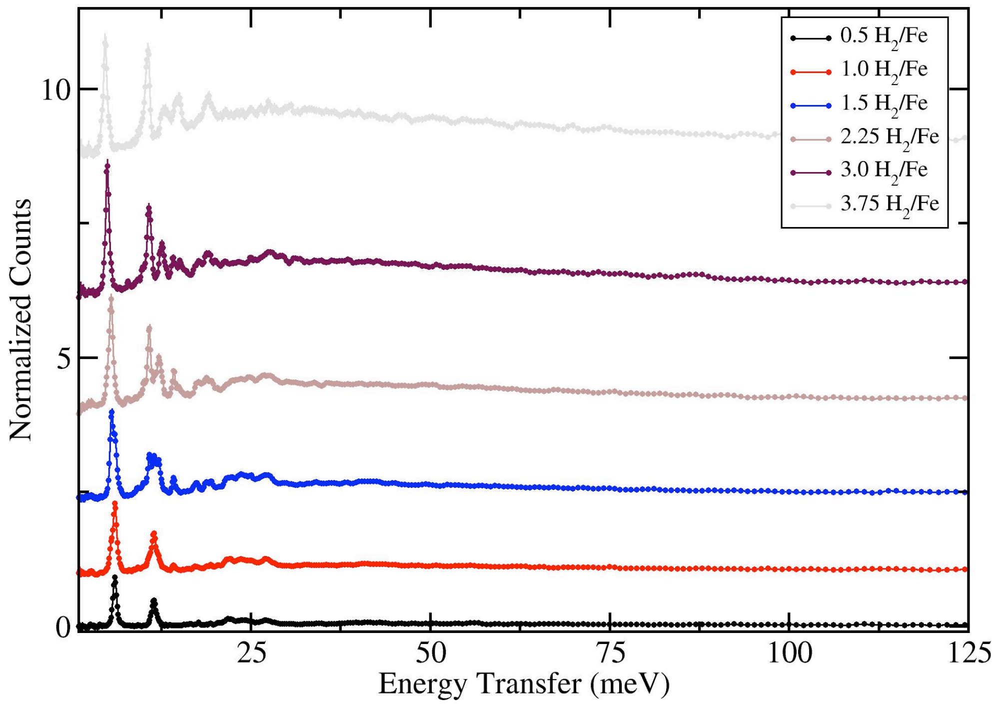

Figure S6: Total integrated intensities of the spectra shown in Figure S5.

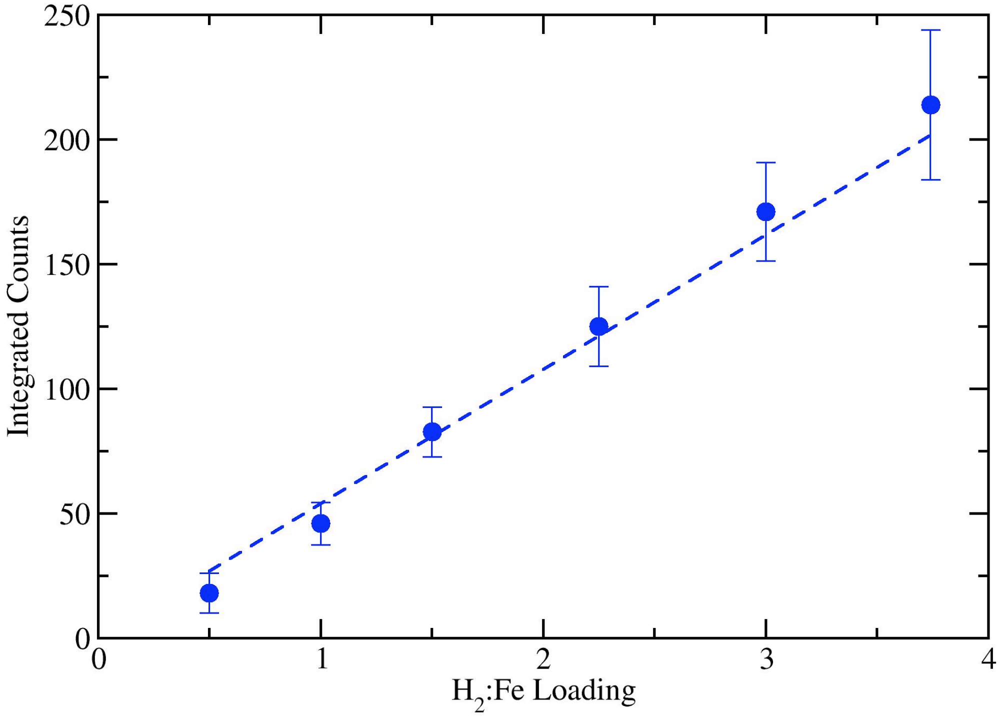

Figure S7: Comparison of the INS spectra of Fe_2(dobdc) and $Fe_2(O_2)$(dobdc) loaded with 0.5, 1.0, and 1.5 *n*-H_2 molecules per Fe^{2+} and Fe^{3+}, respectively. Fe_2(dobdc) is dark blue, red, and black while the spectra obtained from the oxidized derivative are cyan, brown, and grey.

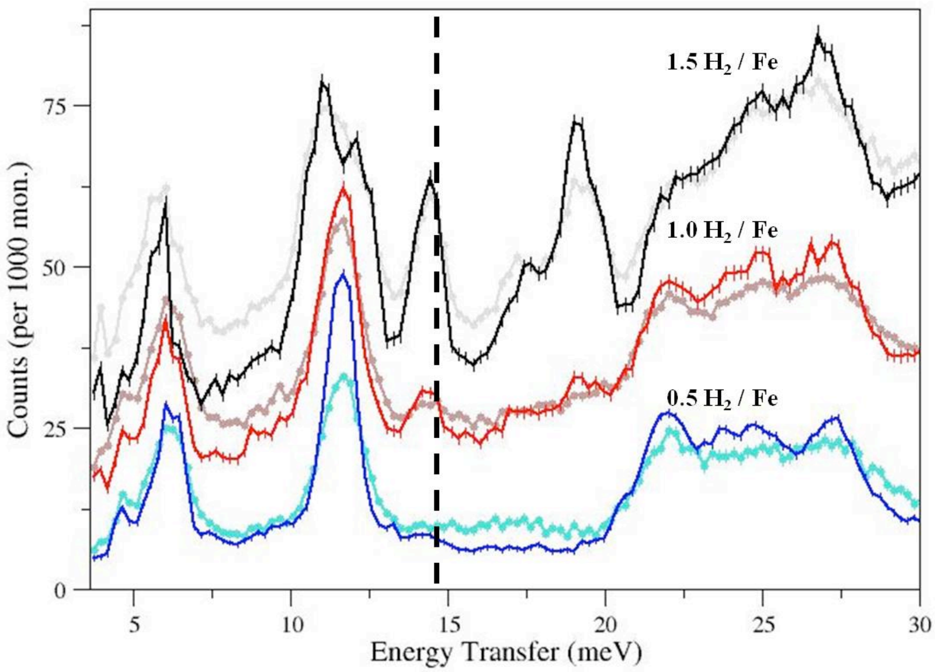

Isosteric Heats of Adsorption Calculations

In order to evaluate different strategies for calculating the isosteric heats of adsorption (Q_{st}) for Fe_2(dobdc) as a function of loading, the isotherm data at 77 and 87 K were fit using three different models. In all cases, Q_{st} was calculated using the Clausius-Clapeyron equation:

$$-Q_{st} = RT^2\left(\frac{\partial \ln p}{\partial T}\right)_n \tag{1}$$

In order to use the Clausius-Clapeyron equation, it is necessary to have equations that describe pressure as a function of loading for at least two different temperatures. Most physically realistic isotherm models give loading as a function of pressure. As such, virial-type equations have been widely used for calculating isosteric heats of adsorption. Typically, Equation 2 is used to fit the adsorption data simultaneously at multiple temperatures.

$$\ln p = \ln n + \left(\frac{1}{T^2}\right)\sum_{i=0}^{j} a_i n^i + \sum_{i=0}^{k} b_i n^i \tag{2}$$

By applying Equation 1, Q_{st} can be easily calculated from this virial model at any loading. Additionally, the zero-coverage isosteric heat of adsorption can be calculated directly from a_0.

$$-Q_{st} = -R\sum_{i=0}^{j} a_i n^i \tag{3}$$

The H_2 adsorption isotherm data at 77 and 87 K for Fe_2(dobdc) were fit simultaneously in OriginPro 8 using Equation 2. The fitted parameters are summarized in Table S9. The final fit did not improve by adding additional a or b parameters. The quality of the fits was evaluated by comparing the adjusted R^2 and residual sum of squares, and by visual inspection. In all cases, significant deviations were observed between the virial model and the experimental data, especially near the inflection that occurs in the isotherms as the exposed Fe^{2+} sites become saturated.

In an effort to get better agreement between the isotherm model and experimental data, the more physically realistic dual-site Langmuir model (Equation 4) was used to independently fit the 77 and 87 K isotherm data for Fe_2(dobdc). Here, n is the amount adsorbed (mmol/g), q_{sat} is the saturation loading for site A or B (mmol/g), b is the Langmuir parameter associated with site A or B (bar^{-1}), and p is the pressure (bar). The fitted parameters are summarized in Table S7.

$$n = \frac{q_{sat,A} b_A p}{1 + b_A p} + \frac{q_{sat,B} b_B p}{1 + b_B p} \tag{4}$$

The isosteric heats of adsorption can be calculated by solving the dual-site Langmuir equations at each temperature for explicit values of *n*. The isosteric heats of adsorption can then be determined using the integrated form of the Clausius-Clapeyron equation (Equation 5) by calculating the slope of ln(p) vs $1/T$ for each loading.

$$(\ln p)_n = \left(\frac{Q_{\mathrm{st}}}{R}\right)\left(\frac{1}{T}\right) + C \tag{5}$$

Significantly, the isosteric heats of adsorption calculated using the virial method and dual-site Langmuir method show different trends as the loading of H_2 is increased. For the virial method, Q_{st} decreases continuously with increasing loading. For the dual-site Langmuir, the isosteric heat of adsorption remains relatively constant until a loading of 4 mmol/g at which point it rapidly decreases. The isosteric heats of adsorption curves are compared in Figure S10. Determining the correct isosteric heats of adsorption is particularly important for applications in H_2 storage in order to design materials that have optimal H_2 binding enthalpies over the entire loading range of interest.

The difference in trends determined from each model can be attributed primarily to differences in the agreement between the experimental and calculated isotherms. While small differences in the quality of the isotherm fits may not seem important, they can have dramatic effects on the shape of the isosteric heat of adsorption curves, especially at lower loadings. Based on visual inspection and comparison of statistical parameters, the viral and dual-site Langmuir methods described above seem to both give very good descriptions of the experimental isotherms. However, when the isotherms and corresponding fits are plotted on a log-scale, significant differences in the quality of the fits become obvious (Figure S8). Specifically, the virial method does not adequately model the inflection that occurs in the isotherm data. As a result, the calculated isosteric heat of adsorption is under-estimated at pressures between approximately 10^{-3} and 10^{-1} bar.

Additionally, the isotherm data for Fe_2(dobdc) were fit independently at 77 and 87 K using a different virial-type equation:

$$\ln p = \ln n + \sum_{i=0}^{j} a_i n^i \tag{6}$$

The isotherms calculated based on these fits showed significantly better agreement than those calculated from fitting to Equation 2. The fit parameters are summarized in Table S10. The resulting isosteric heat of adsorption curve shows a similar trend to that calculated using the dual-site Langmuir model. The oscillations at loadings below 6 mmol/g are likely a result of difficulties in fitting the steep initial rise and inflection in the isotherm data with a virial-type equation.

In summary, the isosteric heats of adsorption calculated using the dual-site Langmuir model seem to be more reasonable based on the better agreement between the experimental and calculated isotherms. Moreover, the trends in isosteric heat of adsorption as a function of loading for the dual-site Langmuir calculations are more physically realistic based on a simple Boltzmann distribution argument. For two sites with an energy difference of 5 kJ/mol (approximately the difference between the strongly adsorbing Fe^{2+} and weak adsorption sites on the pore surface), the population of the higher energy, or weak adsorption sites, is expected to be less than 0.04% at 77 K. As such, it seems reasonable to expect the isosteric heat of adsorption to remain constant until population of the Fe^{2+} sites nears saturation.

For $Fe_2(O_2)$(dobdc), the H_2 adsorption isotherms at 77 and 87 K were independently fit with a dual-site Langmuir-Freundlich model (Equation 7). The fitted parameters are giving in Table S8. The α terms were necessary to get good agreement with the experimental isotherm data. Isosteric heats of adsorption were calculated using Equation 5 as described above and are show in Figure S12.

$$n = \frac{q_{\mathrm{sat,A}} b_{\mathrm{A}} p^{\alpha_A}}{1 + b_{\mathrm{A}} p^{\alpha_A}} + \frac{q_{\mathrm{sat,B}} b_{\mathrm{B}} p^{\alpha_B}}{1 + b_{\mathrm{B}} p^{\alpha_B}} \tag{7}$$

Figure S8: H_2 adsorption isotherms for Fe_2(dobdc) at 77 K (blue) and 87 K (red) with the corresponding dual-site Langmuir (DSL, black) and virial fits (green). For the virial method, the 77 and 87 K data were fit simultaneously with Equation 2. The virial fit does not adequately model the inflection in the isotherm data.

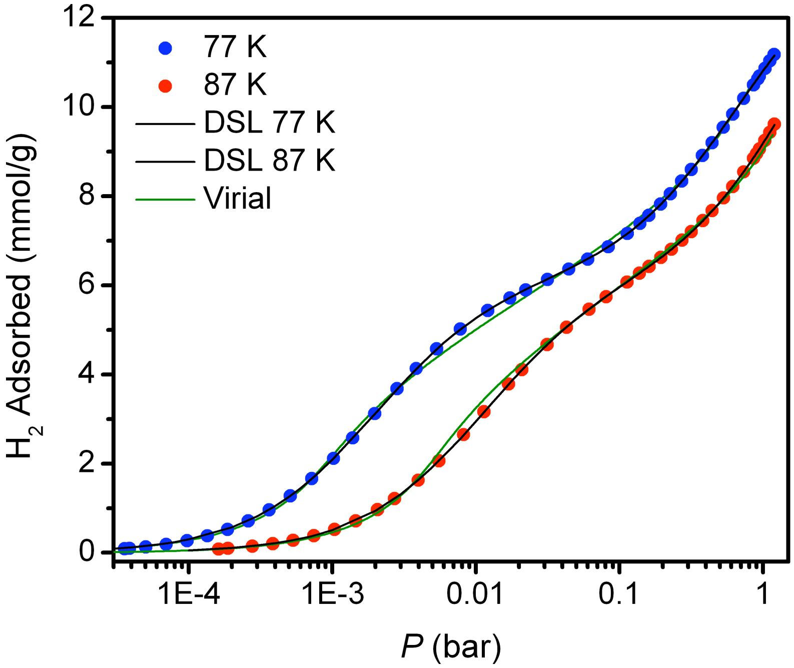

Figure S9: H_2 adsorption isotherms for Fe_2(dobdc) at 77 K (blue) and 87 K (red) with the corresponding dual-site Langmuir (DSL, black) and independently virial fits (purple). For this virial method, the 77 and 87 K data were fit independently with Equation 6.

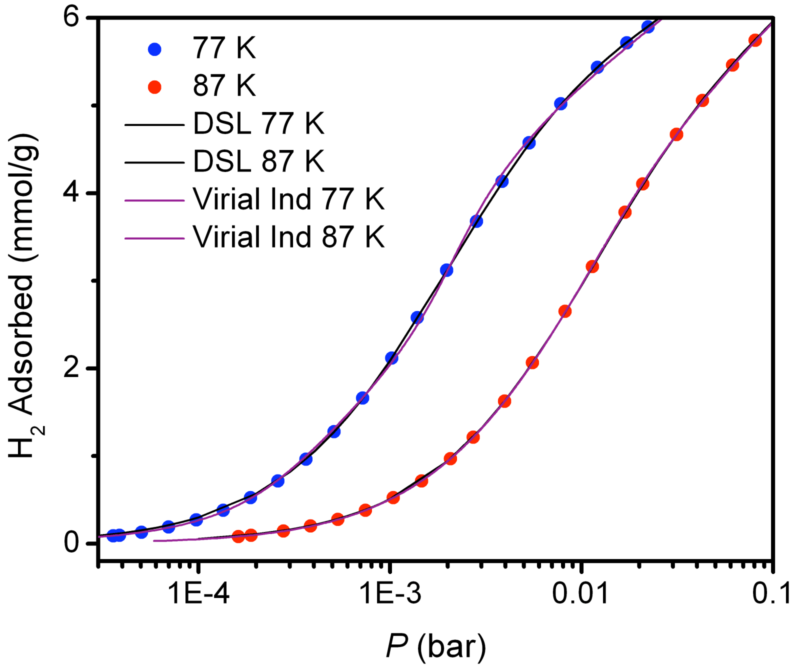

Figure S10: Isosteric heats of adsorption (-Q_{st}) for Fe_2(dobdc) as a function of loading as calculated from the dual-site Langmuir (green), virial (red), and independent virial (blue) fits.

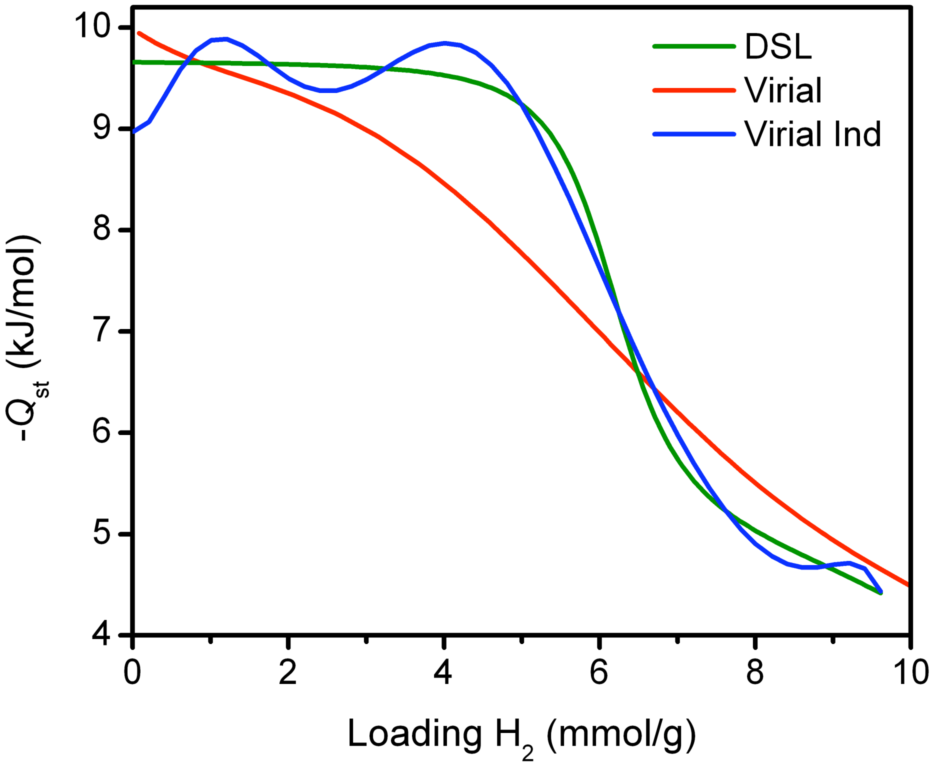

Figure S11: H_2 adsorption isotherms for $Fe_2(O_2)$(dobdc) at 77 K (blue) and 87 K (red) with the corresponding dual-site Langmuir-Freundlich (DSLF, black).

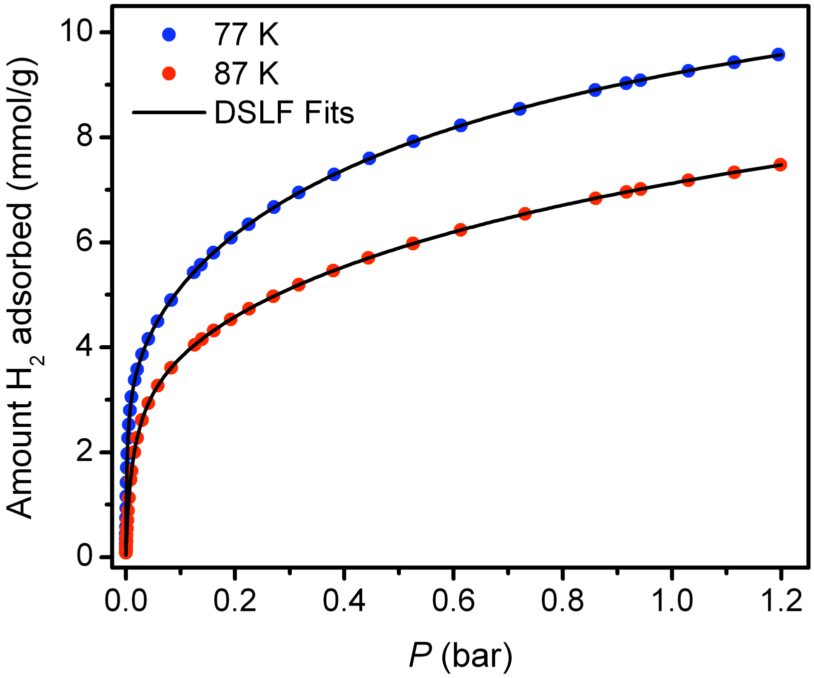

Figure S12: Comparison of isosteric heats of adsorption as a function of loading as calculated for Fe_2(dobdc) (green) and $Fe_2(O_2)$(dobdc) (blue).

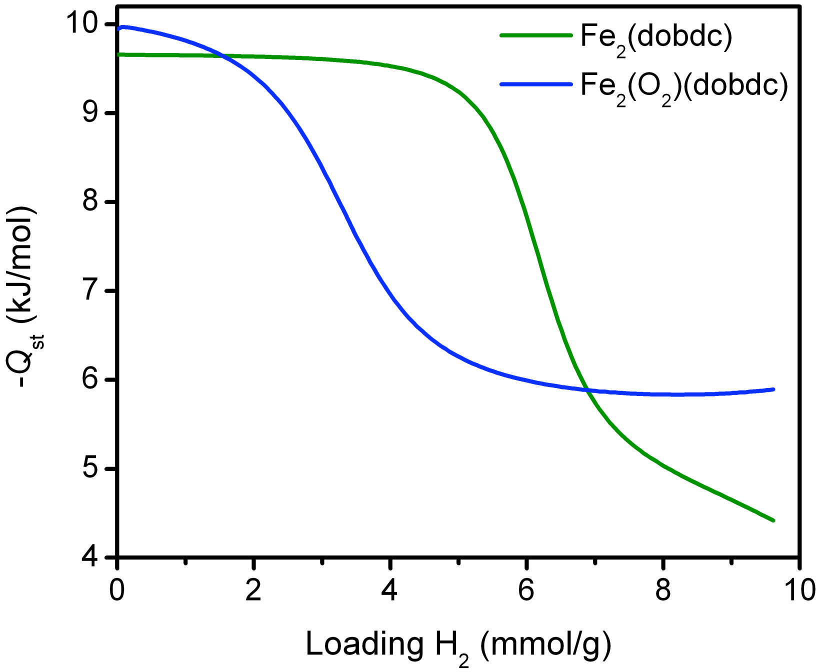

Table S7: Dual-site Langmuir parameters for H_2 adsorption in Fe_2(dobdc) at 77 and 87 K.

	77 K	87 K
$q_{\mathrm{sat,a}}$	6.2	6.1
$q_{\mathrm{sat,b}}$	7.9	9.7
b_{a}	509	0.476
b_{b}	1.43	89.8

Table S8: Dual-site Langmuir-Freundlich parameters for H_2 adsorption in $Fe_2(O_2)$(dobdc) at 77 and 87 K.

	77 K	87 K
$q_{\mathrm{sat,a}}$	3.0	3.0
$q_{\mathrm{sat,b}}$	11.6	11.0
b_{a}	347	64.2
b_{b}	1.14	0.601
α_{a}	0.94	0.94
α_{b}	0.69	0.72

Table S9: Virial parameters for H_2 adsorption in Fe_2(dobdc) at 77 and 87 K. The isotherm data at each temperature were fit simultaneously using Equation 2.

	77 and 87 K
a_0	−1201.20808
a_1	63.1327
a_2	−26.46744
a_3	8.713
a_4	−0.92219
a_5	0.03186
b_0	7.55067
b_1	−0.32577

Table S10: Virial parameters for H_2 adsorption in $Fe_2(dobdc)$ at 77 and 87 K. The isotherm data at each temperature were fit independently using Equation 6.

	77 K	87 K
a_0	−7.84569	−6.23419
a_1	−0.09388	−0.15749
a_2	0.40798	0.49647
a_3	0.76082	−0.39498
a_4	−0.43596	0.19638
a_5	0.12333	−0.06097
a_6	−0.01911	0.01175
a_7	0.00165	−0.00134
a_8	-7.531×10^{-5}	8.116×10^{-5}
a_9	1.406×10^{-6}	-2.024×10^{-6}